Petroleum Science 20 (2023) 982–992

Contents lists available at ScienceDirect

Petroleum Science

journal homepage: www.keaipublishing.com/en/journals/petroleum-science

Original Paper

A novel triple responsive smart fluid for tight oil fracturing-oil expulsion integration

Ming-Wei Gao [a, b, c], Ming-Shan Zhang [c], Heng-Yi Du [d], Ming-Wei Zhao [a, b], Cai-Li Dai [a, b, **], Qing You [e, ***], Shun Liu [d, *], Zhe-Hui Jin [c]

[a] Shandong Key Laboratory of Oilfield Chemistry (China University of Petroleum (East China)), Qingdao, 266580, Shandong, PR China
[b] Key Laboratory of Unconventional Oil & Gas Development (China University of Petroleum (East China)), Ministry of Education, Qingdao, 266580, Shandong, PR China
[c] Department of Civil and Environmental Engineering, University of Alberta, Edmonton, Alberta, T6G 1H9, Canada
[d] Shaanxi Key Laboratory of Advanced Stimulation Technology for Oil & Gas Reservoirs, Engineering Research Center of Development and Management for Low to Ultra-low Permeability Oil & Gas Reservoirs in West China (Ministry of Education), Xi'an Shiyou University, Xi'an, 710065, Shaanxi, PR China
[e] School of Energy Resources, China University of Geosciences, Beijing, 100083, PR China

ARTICLE INFO

Article history:
Received 11 February 2022
Received in revised form
4 January 2023
Accepted 9 January 2023
Available online 14 January 2023

Edited by Yan-Hua Sun

Keywords:
Fracturing-oil expulsion integration
Tight oil
Triple responsive smart fluid
"Pseudo-gemini" zwitterionic surfactant
Fracturing fluid
Spontaneous imbibition

ABSTRACT

The traditional multi-process to enhance tight oil recovery based on fracturing and huff-n-puff has obvious deficiencies, such as low recovery efficiency, rapid production decline, high cost, and complexity, etc. Therefore, a new technology, the so-called fracturing-oil expulsion integration, which does not need flowback after fracturing while making full use of the fracturing energy and gel breaking fluids, are needed to enable efficient exploitation of tight oil. A novel triple-responsive smart fluid based on "pseudo-Gemini" zwitterionic viscoelastic surfactant (VES) consisting of *N*-erucylamidopropyl-*N*,*N*-dimethyl-3-ammonio-2-hydroxy-1-propane-sulfonate (EHSB), *N*,*N*,*N*′,*N*′-tetramethyl-1,3-propanediamine (TMEDA) and sodium *p*-toluenesulfonate (NaPts), is developed. Then, the rheology of smart fluid is systematically studied at varying conditions (CO_2, temperature and pressure). Moreover, the mechanism of triple-response is discussed in detail. Finally, a series of fracturing and spontaneous imbibition performances are systematically investigated. The smart fluid shows excellent CO_2-, thermal-, and pressure-triple responsive behavior. It can meet the technical requirement of tight oil fracturing construction at 140 °C in the presence of 3.5 MPa CO_2. The gel breaking fluid shows excellent spontaneous imbibition oil expulsion (~40%), salt resistance (1.2×10^4 mg/L Na^+), temperature resistance (140 °C) and aging stability (30 days).

1. Introduction

Due to the growing global energy consumption (Wang et al., 2017) and the continuous depletion of conventional oil reservoirs (Wei et al., 2017; Baragau et al., 2021), tight oil has become an important source of oil supply (Wei et al., 2020; Zhang et al., 2022a). Tight porous media is associated with ultra-low permeability and porosity as well as poor connectivity (Miskimins, 2009; Zhou et al., 2020), due to the presence of a significant amount of nanometer and micrometer sized pores (Wang et al., 2019; Li W. et al., 2021), resulting in enormous challenges in tight oil exploitations (Kim et al., 2017). In contrast to the conventional oil reservoirs, in tight porous media, hydraulic fracturing is an imperative development method, which can generate fractures to form a complex oil flow network along with natural fractures (Wu et al., 2018a; Zhang et al., 2022b).

The characteristics and functionality of fracturing fluids are essential to the success of hydraulic fracturing (Zhang Y. et al., 2018). For traditional polymer fracturing fluids such as guar gum and acrylamide polymers, insoluble residue can cause serious damage to the formation by plugging pore throats (Holtsclaw and

* Corresponding author.
** Corresponding author. Shandong Key Laboratory of Oilfield Chemistry (China University of Petroleum (East China)), Qingdao, 266580, Shandong, PR China.
*** Corresponding author.
E-mail addresses: daicl@upc.edu.cn (C.-L. Dai), youqing@cugb.edu.cn (Q. You), liushun631@163.com (S. Liu).

https://doi.org/10.1016/j.petsci.2023.01.008

Funkhouser, 2010; Kong et al., 2017). In addition, the incomplete gel breaking is also detrimental to fracturing operations (Ellis, 1998; Holtsclaw and Funkhouser, 2010). Upon the completion of fracturing construction, flowback should take place as soon as possible to reduce damage to the reservoir (Rassenfoss, 2011), which wastes both energy (high pressure) and chemicals (fracturing fluids) injected into the formation. The generation of a large quantity of flowback water with chemical residues from fracturing fluids and dissolved minerals poses serious environmental concerns (Kong et al., 2017). On the other hand, tight oil production rates tend to decline rapidly, which greatly hamper exploitation and development activities (Hua et al., 2020). If only horizontal and hydraulic fracturing techniques are applied, the average tight oil recovery is typically less than 10% (Sheng et al., 2017). As an enhanced oil recovery (EOR) method, water huff-n-puff, which can replenish formation energy and facilitate spontaneous imbibition, has been proven to be an effective method to improve tight oil recovery (Sheng, 2020). A number of studies and field tests have been carried out on tight oil fracturing and huff-n-puff (Samuel et al., 1997; Heitmann et al., 2001; Lu et al., 2017; Sheng et al., 2017; Wu et al., 2018a; Sheng, 2020). However, the traditional multi-process for tight oil EOR relying on fracturing and huff-n-puff have obvious deficiencies, such as high cost, complex process, and resource-wasting, *etc.* (Peng et al., 2019; Liu et al., 2020). Therefore, a new technology, the so-called fracturing-oil expulsion integration, must be employed to further open the blocking, which can simplify recovery process, reduce cost, and protect the environment, *etc.* (Dai et al., 2020). The fracturing-oil expulsion integration means that the well is shut-in immediately after fracturing without flowback, while it is directly opened for production after shut-in (Zhou et al., 2019). The working fluids used should have excellent fracture-making and sand-carrying ability without residue and induce little damage after gel breaking (Mao et al., 2018). Meanwhile, the gel breaking fluid should have excellent interfacial activity and realize oil-water replacement through spontaneous imbibition during shut-in (Dai et al., 2015). Since there is no flowback after fracturing, the fracturing energy is completely used to supplement the formation performance (Zhou et al., 2019). Therefore, the fracturing-oil expulsion integration can not only meet the needs of tight formation fracturing, but also make full use of fracturing energy and gel breaking fluids for tight oil EOR (Liu et al., 2020).

In recent decades, viscoelastic surfactant (VES) fracturing fluids, which often utilize small molecules and are free of residues have drawn extensive attention as an alternative to polymer-based fracturing fluids (Samuel et al., 1997; Heitmann et al., 2001; Lu et al., 2017). VES fracturing fluids cause minimal damages to the formations and can be easily prepared. In addition, they can break gel thoroughly and rapidly return to low-viscosity spherical micelles, when in contact with the underground hydrocarbons (Crews, 2005; Lerouge and Berret, 2010). The gel-breaking VES fracturing fluids have shown enormous potentials in tight oil development (Dai et al., 2015; Huang et al., 2021). Nevertheless, severe adsorption, high dosage and poor heat resistance greatly limit the applications of traditional VES fracturing fluids in tight formations (Mao et al., 2018; Gao et al., 2022). The Gemini surfactants, consisting of two single-chain surfactants linked by a spacer group, have superior self-assembly properties compared to the single-chain surfactants and better rheological behavior (Menger and Keiper, 2000; Nagarajan 2002). A number of heat-resistant novel cationic Gemini VESs (Mao et al., 2016; Yang et al., 2017a, b; Mao et al., 2018; Zhang W. et al., 2018; Xu et al., 2021) with erucamidopropyl (C25) hydrophobic tails and different spacer groups have been synthesized, which generally outperform single-chain VES fracturing fluids. However, Gemini cationic VES fracturing fluids exhibit weak salinity tolerance and severe adsorption (Khair et al., 2011), which is not conducive to spontaneous imbibition and oil expulsion after hydraulic fracturing. Thus, Gemini zwitterionic VESs have drawn great interests among scientists and engineers thanks to their superior properties, including higher thermal stability, lower adsorption and higher salt tolerance (Lu et al., 2016; Zhang et al. 2019, 2020; Wang et al., 2020). For example, Zhang et al. (2020) developed a novel benzene sulfonic Gemini zwitterionic VES (EDBS), which showed superior thermo-shearing in 25% standard brine solution at 120 °C. While these experimental studies have displayed the great promise of Gemini zwitterionic VESs, the complicated synthesis routes, low yield, and high costs still significantly impede their development and industrial applications (Li Z. et al., 2021). Thus, a simple method to synthesize VES, which have a similar performance to Gemini zwitterionic VESs, becomes highly desirable, especially for VES fracturing fluids. Recently, Feng and his coworkers proposed a "pseudo-Gemini" concept to construct CO_2- and pH-responsive viscoelastic fluids (Chu and Feng, 2010; Zhang et al., 2013; Feng and Chu, 2015). It opens up a new facile approach to construct VES fracturing fluids using non-covalent interactions and appropriate building blocks. A series of viscoelastic fluids based on "pseudo-Gemini" VES have been developed (Zhang et al., 2016; Wu et al., 2018b; Yang et al., 2019), presenting a great potential in tight oil EOR. As temperature increases, CO_2 is continuously released from the aqueous solution, reversing the reaction and reducing the amine protonation. Meanwhile, CO_2 solubility in water is also affected by its partial pressure. High-temperature and high-pressure conditions in tight oil reservoirs often impose adverse impacts on the performance of fracturing fluids. Therefore, a new high pressure thickening VES fluid is in demand in order to overcome the shortcomings of the existing CO_2-responsive viscoelastic fluid systems.

Hence, in this work, we develop a novel CO_2-, temperature- and pressure-triple responsive smart fluids based on "pseudo-Gemini" zwitterionic VESs, which can not only meet the needs of tight oil fracturing construction, but also make full use of fracturing energy and gel breaking fluids, thereby achieving fracturing-oil expulsion integration. The smart fluids are formed by mixing *N*-erucylamidopropyl-*N*,*N*-dimethyl-3-ammonio-2-hydroxy-1-propane-sulfonate (EHSB), *N*,*N*,*N*′,*N*′-tetramethyl-1,3-propanediamine (TMEDA) and sodium *p*-toluenesulfonate (NaPts) without complex organic synthesis. Then, the CO_2-, thermal-, and pressure-responsive behavior of this smart fluid are studied based on its rheological properties. Moreover, the mechanism of triple-responsive smart fluids is discussed in detail. Finally, a series of fracturing and spontaneous imbibition performances are systematically investigated. It is expected that this triple-responsive smart fluid would provide a new idea for the efficient development and exploitation of tight oil reservoirs.

2. Materials and methods

2.1. Materials

EHSB was prepared according to the reference reported by Chu and Feng (2013). And the reaction process is shown in Scheme S1 (Supplementary Material). Sodium *p*-toluenesulfonate (NaPts, ≥96%) and *N*,*N*,*N*′,*N*′-tetramethyl-1,3-propanediamine (TMEDA, ≥99%) are obtained from Aladdin Reagent Co., Ltd. (Shanghai, China) and used without further purification. Shengli tight oil are obtained from Petroleum Engineering Technology Research Institute of Shengli Oilfield. The simulation oil used in this study is a mixture of Shengli tight oil and kerosene (volume ratio: 3:7). The oil density is 0.804 g/cm^3, and its dynamic viscosity is ~5.0 mPa s at 25 °C. The cores are all obtained from Haian Oil Scientific Research

Table 1
The core parameters.

Number	Length, cm	Diameter, cm	Permeability, mD	Porosity, %
1	3.33	2.50	0.120	13.24
2	3.31	2.51	0.117	13.54
3	3.28	2.50	0.112	13.29
4	3.30	2.49	0.113	13.08
5	3.24	2.51	0.119	13.69
6	3.29	2.50	0.109	13.45

Apparatus Co., Ltd and their properties are listed in Table 1.

2.2. Sample preparation

Deionized water is added to a mixture system consisting of EHSB, NaPts, and TMEDA at 60 °C until completely dissolved and equilibrated in a 25 °C thermostatic bath for 72 h.

2.3. Rheological measurements

The rheological properties are measured by a HAAKE MARS60 rheometer (Thermo Fisher, Germany). Prior to the studies, the samples are stabilized in a cylinder at 25 °C for at least 15 min. Steady and dynamic rheological measurements under atmospheric pressure are conducted on a coaxial cylindrical sensor system, which is equipped with a Z43 cup and a CC31/Ti cylinder rotor. Complementary, a high-temperature and high-pressure sealing unit with a D400/300 pressure cell and a PZ37 cylinder rotor are used to study the steady rheological properties under 3.5 MPa CO_2 pressure.

2.4. ^{1}H NMR measurements

^{1}H NMR spectra are measured on a Bruker AVANCE III HD 400 NMR spectrometer (Bruker, Karlsruhe, Germany). The TMEDA is dissolved in deuterium oxide.

2.5. Gel breaking and core permeability damage test

In this work, kerosene is used as a gel breaker to investigate the gel breaking of smart fluid with a volume ratio of 1.5% (kerosene to smart fluid) at 80 °C. Core flooding experiments are employed to investigate the core permeability damage from gel breaking fluids. First, the core is saturated with formation water and the initial permeability (K_1) is measured by forward brine flooding (1.0 mL/min). To simulate matrix damage during fracturing, the gel breaking fluid is injected into the core in the opposite direction at constant differential pressure of 3.5 MPa for 36 min, and then the core is aged at 80 °C for 2 h. Thereafter, the formation water is re-injected into the core to obtain the core permeability (K_2). The core permeability damage rate (η_d) is given as

$$\eta_d = \frac{K_1 - K_2}{K_1} \times 100\% \tag{1}$$

2.6. Scanning electron microscopy

Scanning electron microscope (SEM) measurements are performed by Quanta 450 (FEI, America). All samples for SEM are conductively coated by spraying Au before scanning.

2.7. Interfacial tension

The oil/water interfacial tension (IFT) is measured by the Texas-500 spinning drop interfacial tensiometer at 80 °C based on Eq. (2) (Bai et al., 2014). All measurements are repeated at least three times.

$$\sigma = 1.2336(\gamma_w - \gamma_o)\omega^2\left(\frac{D}{n}\right)^2, \quad f = \frac{L}{D} \geq 4 \tag{2}$$

where σ is the oil/water IFT (mN/m); γ_w is the density of formation water (0.954 g/mL); γ_o is the density of the simulation oil (0.804 g/mL); ω is the rotational speed (6000 rpm); L is the length of the oil drop, mm; D is the width of the oil drop, mm; n is the refractive index of the water phase; f is the correction factor.

2.8. Spontaneous imbibition

The cores are placed in drying oven at 95 °C for 24 h to remove bound water, and then are saturated with simulation oil as in Dai et al. (2017). Before the imbibition experiment, oil-saturated cores are placed in the Amott cells filled with aqueous solution (gel breaking fluid and brine) at 80 °C and stabilized for 24 h to eliminate the influence of temperature on oil volume. During the spontaneous imbibition process, the discharged oil aggregates into the graduated cylinder at the top of the Amott cells. The resolution of the graduated cylinder is 0.01 mL.

3. Results and discussion

3.1. CO_2 and thermal-responsive behavior

The EHSB synthesized in this work is a long-tail zwitterionic amphiphilic surfactant (Wang et al., 2018). The amide group substantially extends surfactant length. On the other hand, it also has a long unsaturated hydrophobic tail (erucyl, C22) (Kumar et al., 2007). Therefore, EHSB solubility in water is extremely low, while the *cis*-unsaturation leads to a kink in the erucyl tails (Kumar and Raghavan, 2009). To enhance EHSB solubility in water, NaPts is used as an organic hydrotrope. Herein, we study a novel CO_2-, thermal-, and pressure-triple responsive smart fluid consisting of EHSB (4.0 wt%, 71.4 mM), NaPts (0.5%, 25.8 mM) and TMEDA (1.2 wt %, 92.3 mM).

As shown in Fig. 1a, during the steady shear measurements, the initial viscosity of the smart fluid increases significantly after CO_2 injection (from 206,845 to 304,764 mPa s). At 25 °C, its viscosity decreases linearly as the shear rate increases. A shear thinning response can be observed throughout the process, indicating that the smart fluid behaves as a typical elastic gel (Raghavan and Douglas, 2012). At 80 °C, the zero shear viscosity (η_0) of the smart fluid with CO_2 is 14,235 mPa s, which is ~23 times larger than that without CO_2 (620 mPa s). At a low shear rate, their viscosities remain constant, demonstrating great shear resistance. Shear-thinning can be observed as the shear rate increases, indicating the formation of longer wormlike micelles (Lu et al., 2016). The critical shear rate of the smart fluid with CO_2 appears at a much lower shear rate, indicating that the wormlike micelles become longer, fewer branches and stiffer (Raghavan and Douglas, 2012). As temperature increases, the initial viscosity decreases and the smart fluid transforms from hydrogels to wormlike micelles (Han et al., 2019). The micelles also become shorter and more flexible at a higher temperature (Yin et al., 2019).

The dynamic rheological experiments are also conducted. As shown in Fig. 1b, the smart fluid shows the same elastic

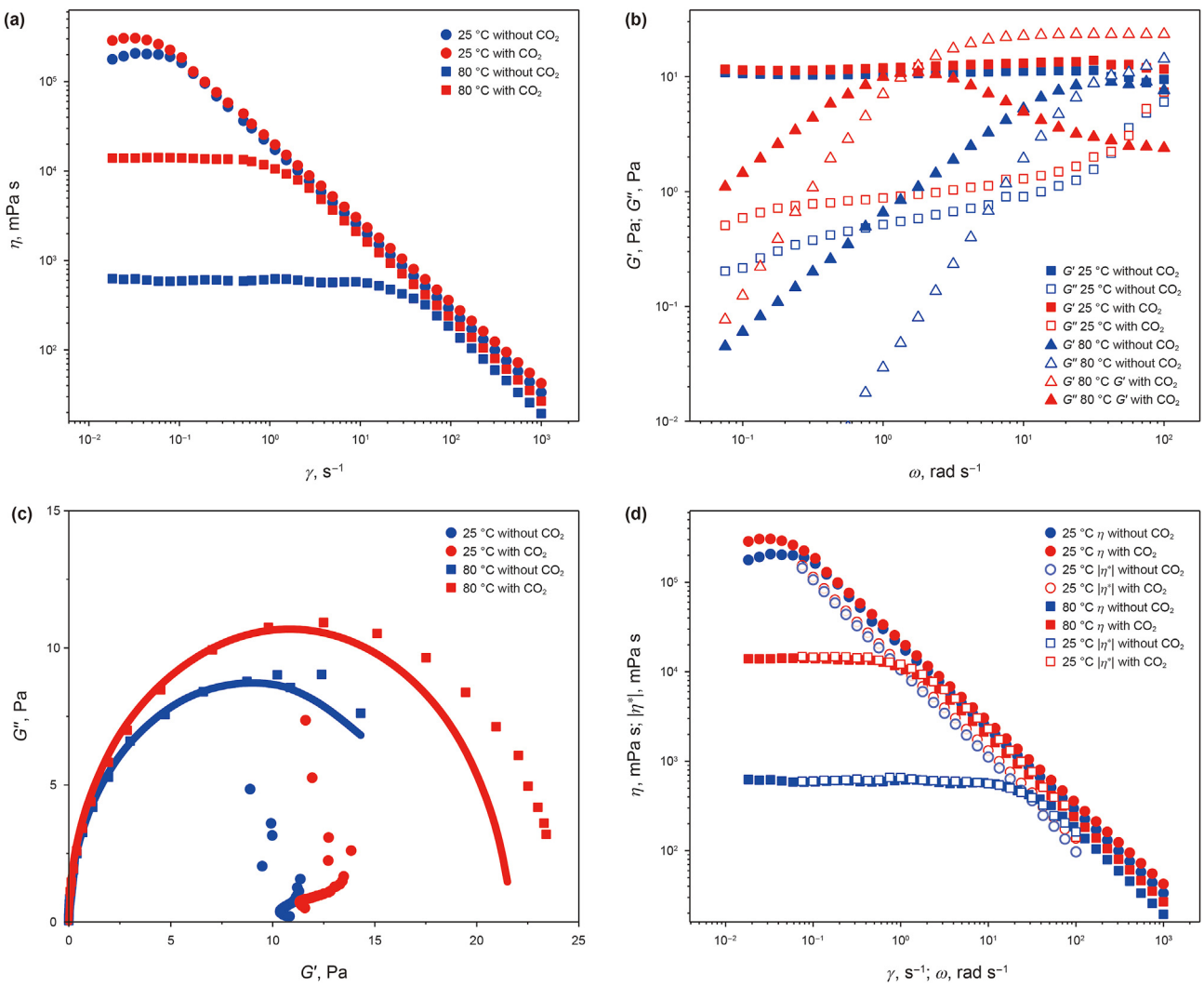

Fig. 1. (**a**) Steady shear viscosity; (**b**) Storage modulus (G') and loss modulus (G'') versus frequency; (**c**) Cole-Cole plot; (**d**) Steady shear viscosity and dynamic complex viscosity of the smart fluids with and without CO_2 at 25 and 80 °C.

performance ($G' > G''$, G' is the storage modulus, G'' is the loss modulus) before/after CO_2 injection at 25 °C. As the frequency increases, G' rises moderately while G'' increases drastically. G' reaches a constant value which is defined as the plateau modulus G'_0 at high frequency. The smart fluid has a higher G'_0 with CO_2, which indicates denser mesh network and longer micelles (Zhao et al., 2017). Therefore, CO_2 injection is beneficial to the formation of elastic gel and network structure, leading to a highly elastic system. At 80 °C, the smart fluid exhibits viscoelastic characteristics. At low frequency, the smart fluid presents viscidity ($G' > G''$), while the elasticity is dominant at high frequency ($G' < G''$). The curves before/after injecting CO_2 are compared against the Maxwell model, which is given as (Granek and Cates, 1992):

$$G'(\omega) = \frac{G'_0 \omega^2 \tau_R^2}{1 + \omega^2 \tau_R^2} \tag{3}$$

$$G''(\omega) = \frac{G'_0 \omega \tau_R}{1 + \omega^2 \tau_R^2} \tag{4}$$

$$\tau_R = \frac{1}{\omega_{CO}} \tag{5}$$

$$G'_0 = 2G^* \tag{6}$$

where ω is the angular frequency; G'_0 is the plateau modulus; τ_R is the relaxation time; ω_{co}, G^* represent the critical angular frequency and modulus, respectively, where the cross of G' and G''. According to this model, the value of the plateau modulus (G'') of micelles provides an estimate for the entanglement length l_e, which is the length of micellar chains in the intervals between the two entanglement points, that can be derived from:

$$G'_0 = 2.446 \times 10^9 \frac{k_B T}{l_e^{9/5}} \tag{7}$$

where k_B is the Boltzmann constant; T is the temperature, K. The network mesh size (ζ_m) can also be estimated from plateau modulus G'_0:

Table 2
Micellar characteristic parameters of different systems.

	T, K	ω_{co}, rad s^{-1}	G'_0, Pa	ξ_m, nm	l_e, nm
With CO_2	353	1.54	23.4	59.28	148.12
Without CO_2	353	31.62	17.4	65.43	174.62

$$G'_0 = \frac{k_B T}{\xi_m^3} \tag{8}$$

According to the above equations, various rheological parameters were calculated and listed in Table 2. After the injection of CO_2, the increases of ξ_m and l_e mean the denser mesh network and longer micelles. The decrease of ω_{co} can be attributed to the microstructural transition induced by temperature, i.e., longer and fewer branches (Lu et al., 2016). To determine whether the smart fluid fits the Maxwell model, the Cole-Cole plot is widely used, which is given as

$$G'^2 + \left(G' - \frac{G'_0}{2}\right)^2 = \left(\frac{G'_0}{2}\right)^2 \tag{9}$$

The Cole–Cole plots for the smart fluid with and without CO_2 at 25 and 80 °C are shown in Fig. 1c. The curve of elastic gel (25 °C) does not show the Maxwell behavior. At 80 °C, the curves with or without CO_2 fit well with the semicircle at low frequency, whereas slightly deviates at high frequency. This phenomenon is consistent with the Maxwell model (Acharya and Kunieda, 2006). The existence of the greater deviation in fluids containing CO_2 indicates a better elasticity.

As shown in Fig. 1d, steady shear viscosity (η) and dynamic complex viscosity ($|\eta^*|$) almost overlap at low shear rates (γ) and frequency (ω), which follows the Cox-Merz rule, at 80 °C (Li et al., 2012). This result reveals the emergence of entanglement among wormlike micelles. At high frequency, the curves start to deviate because of the disintegration of entangled micelles (Miyoshi and Nishinari, 1999). At 25 °C, the two viscosity types are different, i.e., the smart fluids with and without CO_2 have significant elastic characteristics rather than viscoelasticity.

To investigate the thermal endurance of system, the viscosity retention rates (viscosity ratios at 80 and 25 °C) with and without CO_2 are shown in Fig. 2a. As the temperature increases from 25 to 80 °C, η_0 without CO_2 decreases by almost 3 orders of magnitude (viscosity retention rate: 0.3%), while η_0 with CO_2 have only 1 order of magnitude decrease (viscosity retention rate: 4.7%). And the viscosity retention rates with CO_2 at different shear rates are all bigger than that of without CO_2. It indicates that CO_2 injection can not only enhance system rheology, but also significantly improve its temperature resistance. More interestingly, the CO_2-switchability of the rheological properties are reversible by adding and removing CO_2 (to) from the system. Such system reversibility can be repeated numerous times with little changes to system properties (see Fig. 2b). The improved performance of system by adding CO_2 is probably because the protonated amine groups enhance electrostatic interaction.

3.2. Pressure-responsive behavior

It is well known that the CO_2-amine reaction in aqueous solution is a dynamic and reversible process (Heldebrant et al., 2005). As the temperature increases, CO_2 is continuously released from the aqueous solution, reversing the reaction and reducing the amine protonation (Mani et al., 2006). Meanwhile, CO_2 solubility in water is also affected by its partial pressure (Someya et al., 2005). High-temperature and high-pressure conditions in tight oil reservoirs often impose adverse impacts on the performance of fracturing fluids. Hence, the effect of pressure at high temperature conditions on the rheology of CO_2-VES fluid directly determines the quality of fracturing operations, especially during the initiation and proppant delivery stages. In order to minimize the impact of CO_2 release, pressurization process is carried out in a CO_2 atmosphere. As shown in Fig. 3, at 3.5 MPa, the system viscosity shows a linear and sharp decline as the shear rate increases, indicating non-Newtonian fluid behavior and the destruction of gel structures (Bandyopadhyay and Sood, 2003). We note that there is no Newtonian fluid area at low stresses, in contrast to the typical wormlike micellar behavior, indicating the formation of elastic gel (Dong et al., 2008; Yan and Pochan, 2010). The micelle grows rapidly and transforms into elastic gel, as the pressure increases from the atmospheric pressure to 3.5 MPa (Fig. 3) and the viscosity of this VES fluid is dependent on CO_2 pressure.

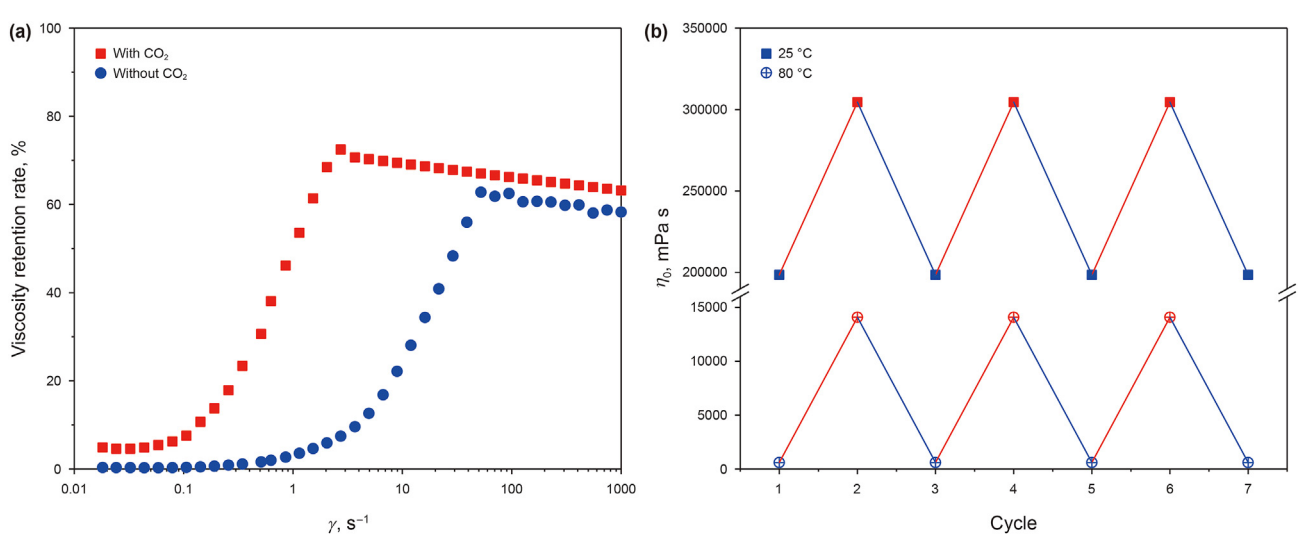

Fig. 2. (**a**) The viscosity retention rates of the smart fluids with and without CO_2; (**b**) Switchable viscosity of the smart fluids at 25 and 80 °C.

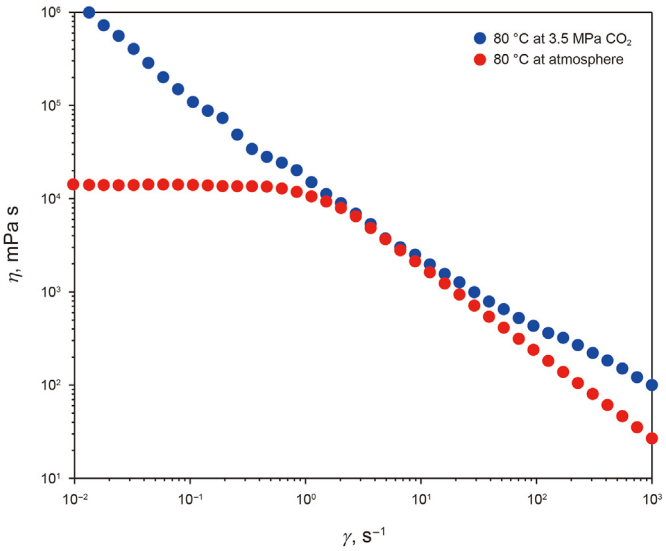

Fig. 3. Steady shear viscosity of the smart fluids with CO_2 for different CO_2 pressure at 80 °C.

3.3. Mechanism of triple responsive smart fluid

This self-assembled structure and its sensitivity to environmental stimuli, such as CO_2, stem from the changes in molecular structures and intermolecular forces. A mechanism is proposed to explain the formation of viscoelastic fluid and its triple smart responsiveness as shown in Fig. 4.

Ultra-long hydrophobic chain (erucamide propyl) endows surfactant molecules with strong self-assembly capabilities and poor water solubility (Kumar and Raghavan, 2009). At room temperature, EHSB solubility in water is small. As a result, it does not have a high aggregation ability. On the other hand, NaPts can form electrostatic pairing with the zwitterionic headgroup of EHSB. The benzyl group of NaPts is embedded vertically in the hydrophobic chains of EHSB, while the sulfonate anion is located close to the positively-charged part of EHSB head group at the hydrophilic polar layer. The adsorption of NaPts not only reduces electrostatic repulsion, but also enhances electrostatic shielding (Mushi et al., 2020). The presence of TMEDA can alter the polarity of H_2O and EHSB, which is conducive to the dissolution of EHSB. In the EHSB/NaPts/TMEDA system, the TMEDA molecules tend to enter micelles through self-assembly with EHSB and NaPts. As a result, under the influence of NaPts and TMEDA, EHSB gradually dissolves in H_2O and self-assembles to form stiff wormlike micelle, i.e., elastic gel (see Fig. 4a).

In order to investigate why the smart fluid shows such different rheological behavior before/after injecting CO_2, ^{1}H NMR of TMEDA is performed and the proton resonances of TMEDA are shown in Fig. 5a. After injecting CO_2, the chemical shifts of protons move from 2.07 (a_1), 2.21 (b_1) and 1.52 (c_1) to 2.27 (a_2) 2.45 (b_2) and 1.68 (c_2), respectively, reflecting the protonation of TMEDA. In other words, TMEDA molecules react with CO_2 to form bola-type ammonium salt, $(CH_3)_2NH^+(CH_2)_3NH^+(CH_3)_2(TMEDAH_2^{2+})$, in aqueous solution. More importantly, the $TMEDAH_2^{2+}$ molecule with two positive charges can link with two zwitterionic VESs by non-covalent electrostatic attraction to form a "pseudo-Gemini" zwitterionic VES, 2EHSB-$TMEDAH_2^{2+}$ (see Fig. 5b). Compared with non-ionic TMEDA molecule, the double protonated $TMEDAH_2^{2+}$ molecule is more hydrophilic and can migrate to the micellar interface, which narrows the gap between the sulfonate anion of EHSB.

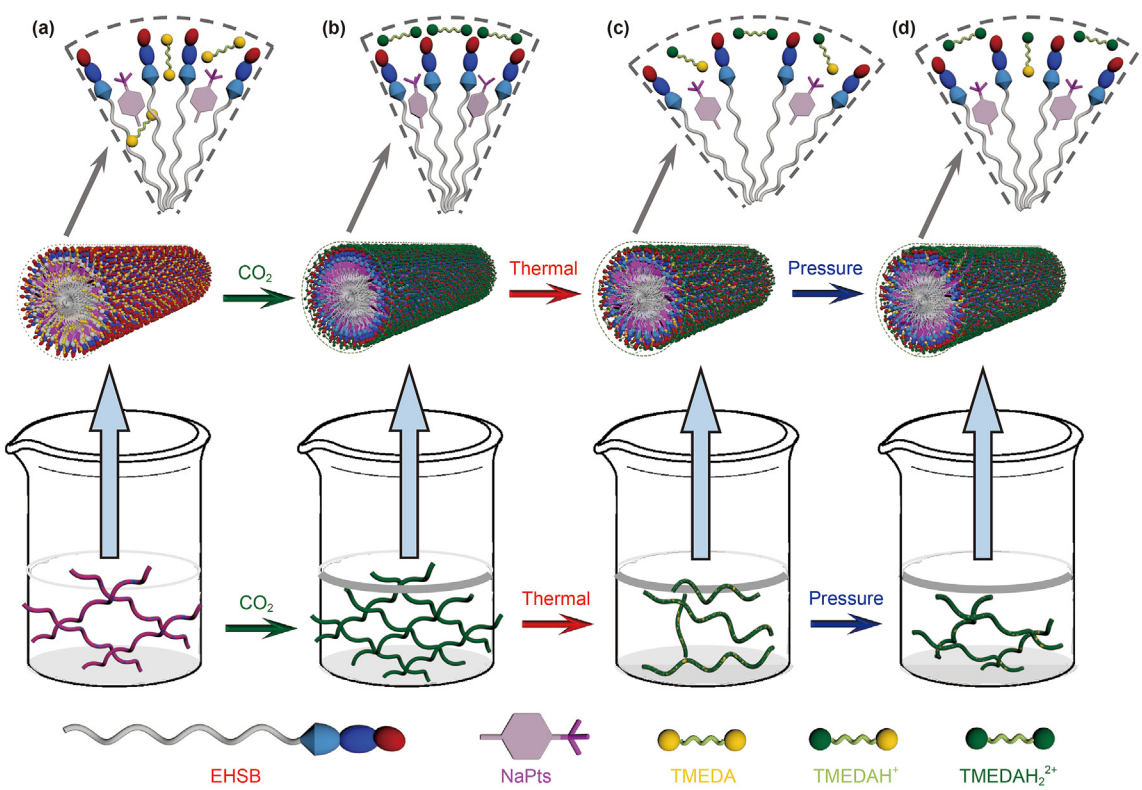

Fig. 4. Schematic illustration of self-assembly mechanism of the smart fluid induced by CO_2, thermal and pressure. (**a**) Elastic gel, initial state without CO_2 at 25 °C and atmosphere; (**b**) Stronger elastic gel, after CO_2-response at 25 °C and atmosphere; (**c**) Wormlike micelle, after CO_2-response at 80 °C and atmosphere; (**d**) Stronger wormlike micelle, after CO_2-response at 80 °C and 3.0 MPa CO_2.

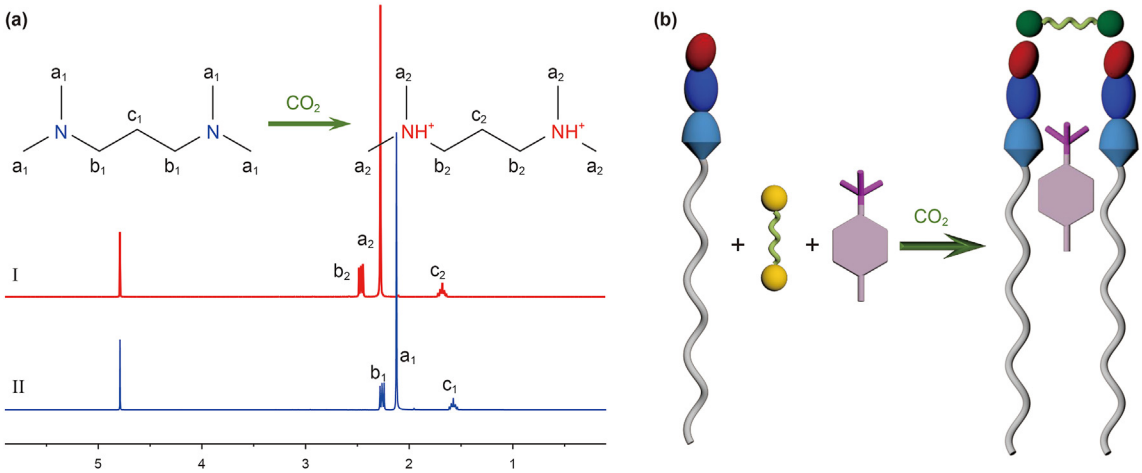

Fig. 5. (**a**) ^{1}H NMR of TMEDA without (a-I) and with (a-II) CO_2; (**b**) Schematic illustration of the possible interaction mechanisms of EHSB, TMEDA and NaPts with CO_2.

Therefore, after injecting CO_2, the wormlike micelle becomes much longer and stiffer, causing the sharp rise in the viscosity, viscous modulus and elastic modulus (see Fig. 4b). On the other hand, due to the "pseudo-Gemini" zwitterionic VES, the thermal endurance of the system with CO_2 is significantly superior than that without CO_2.

As the temperature increases, the reaction between TMEDA and CO_2 proceeds in the opposite direction, i.e., the degree of TMEDA protonation decreases. In addition, the temperature can also affect the non-covalent interactions and molecular thermal motion (Wu et al., 2018). At a higher temperature, surfactant molecules spend less time on their end-caps due to the rapid exchange. Consequently, additional end-caps can be generated, resulting in shorter micelles. Hence, less protonation of TMEDA, weaker non-covalent interaction and stronger thermal motion lead to the rapid decrease in viscosity upon heating (see Fig. 4c). As the CO_2 partial pressure increases, more CO_2 molecules are dissolved in the aqueous solution which enhances protonation of TMEDA, resulting in a higher viscosity (see Fig. 4d).

3.4. Fracturing fluid functional performances

3.4.1. Temperature and shear resistance

In actual hydraulic fracturing, the high temperature and high shear in the wellbore may result in sharp decreases in fracturing fluid viscosity. Therefore, excellent temperature and shear resistance is necessary for the fracturing fluid to create joints and carry proppant. We increase the system temperature from 25 to 140 °C at a rate of 3 °C/min with continuous shearing at 170 s^{-1} for 7000 s to simulate the actual fracturing process. As shown in Fig. 6, when the pressure cell is filled with 3.5 MPa CO_2, the fluid viscosity increases to ~30 mPa s, which can satisfy field application requirement.

3.4.2. Gel breaking and core permeability damage performance

In order to reduce formation damage and achieve high reservoir productivity, fracturing fluid should be broken as soon as possible after fracturing construction. Compared with traditional polymer fracturing fluid, VES fluids automatically break the gel when it meets oil (alkane), while no additional breaker is needed. For conventional fracturing fluids (nanoparticle-enhanced supramolecular fracturing fluid, NESF and crosslinked guar fracturing fluid, CGF), there are some residual gel and residue in their gel breaking fluids and the residue can adsorb on the surface of the crack (Huang et al., 2021). The gel breaking fluid of the new system has no residue and its viscosity is ~1 mPa s after adding kerosene (1.2%) at 80 °C.

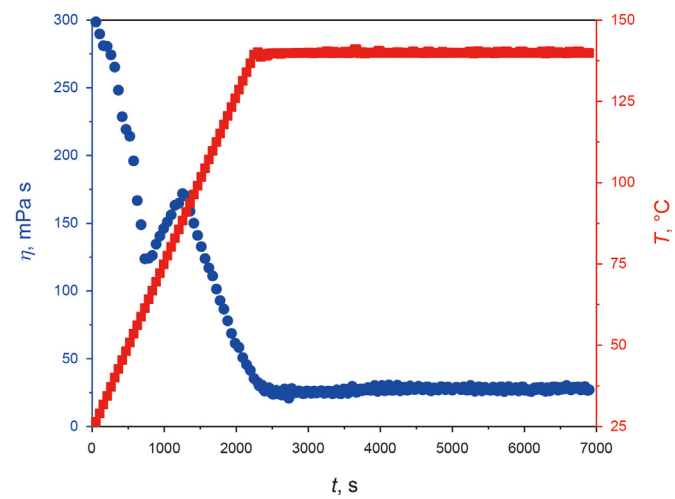

Fig. 6. Apparent viscosity (170 s^{-1}) and temperature as a function of time for the smart fluids with CO_2 at 3.5 MPa CO_2 pressure.

Table 3
The damage of core permeability by gel breaking fluid.

Number	Initial permeability, mD	Final permeability, mD	η_d, %
1	0.120	0.116	3.33

The average core permeability damage caused by NESF is 22.57%, which is similar to core permeability damage caused by CGF (Huang et al., 2021). As shown in Table 3, the permeability damage rate of the new system (3.33%) is lower than NESF and CGF, indicating that the gel breaking liquid incurs minimal damage to the core.

3.5. Spontaneous imbibition of gel breaking fluids

The oil recovery for gel breaking fluid during spontaneous imbibition is plotted in Fig. 7. All imbibition oil recovery curves show a similar trend. The oil recovery of gel breaking fluid increases throughout the oil production process. The oil recovery increases significantly for the first 12 h and subsequently reaches a plateau from 12 to 60 h. Then, when the imbibition period passes 60 h, the volume tends to stay constant, indicating that very little or no water

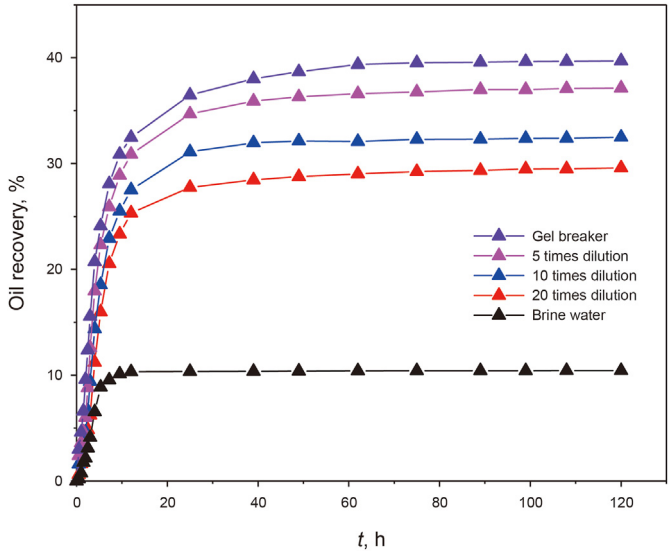

Fig. 7. Oil recoveries of spontaneous imbibition experiments for gel breaking fluids and brine water at 80 °C.

imbibes into the rock cores. As the breaking gel becomes more dilute, the oil recovery decreases slightly. The gel breaking fluid has the best oil displacement performance (i.e., ~40%). The dilution effect of the formation water reduces the spontaneous imbibition of breaking fluid, but the oil recovery of the diluted breaking fluid still reaches ~24%, which is significantly higher than the oil recovery of brine (~10%), NESF (~19%), and CGF (~8%) (Huang et al., 2021).

We also study the effect of temperature and salinity on the stability of gel breaking fluid. Gel breaking fluid is placed into water bath at 30, 40, 50, 60, 70, and 80 °C, respectively. The IFT between simulation oil and gel breaking fluid at different temperatures is shown in Fig. 8a. As the temperature increases, IFT decreases moderately. At temperature higher than 40 °C, IFT remains constant, indicating that the breaking gel presents a good temperature resistance. To further investigate whether the gel breaking fluids can withstand high temperature for a long time, the fluid is sealed into ampoule bottle and placed in a thermostat at 80 °C for a month. Then, IFT is measured and recorded every 5 day as shown in Fig. 8b. As the aging time increases, the breaking gel transforms from colorless and transparent to yellow (see Fig. 8d), while IFT remains almost constant, indicating a great temperature resistance. To study the effect of salinity on simulation oil-gel breaking fluid

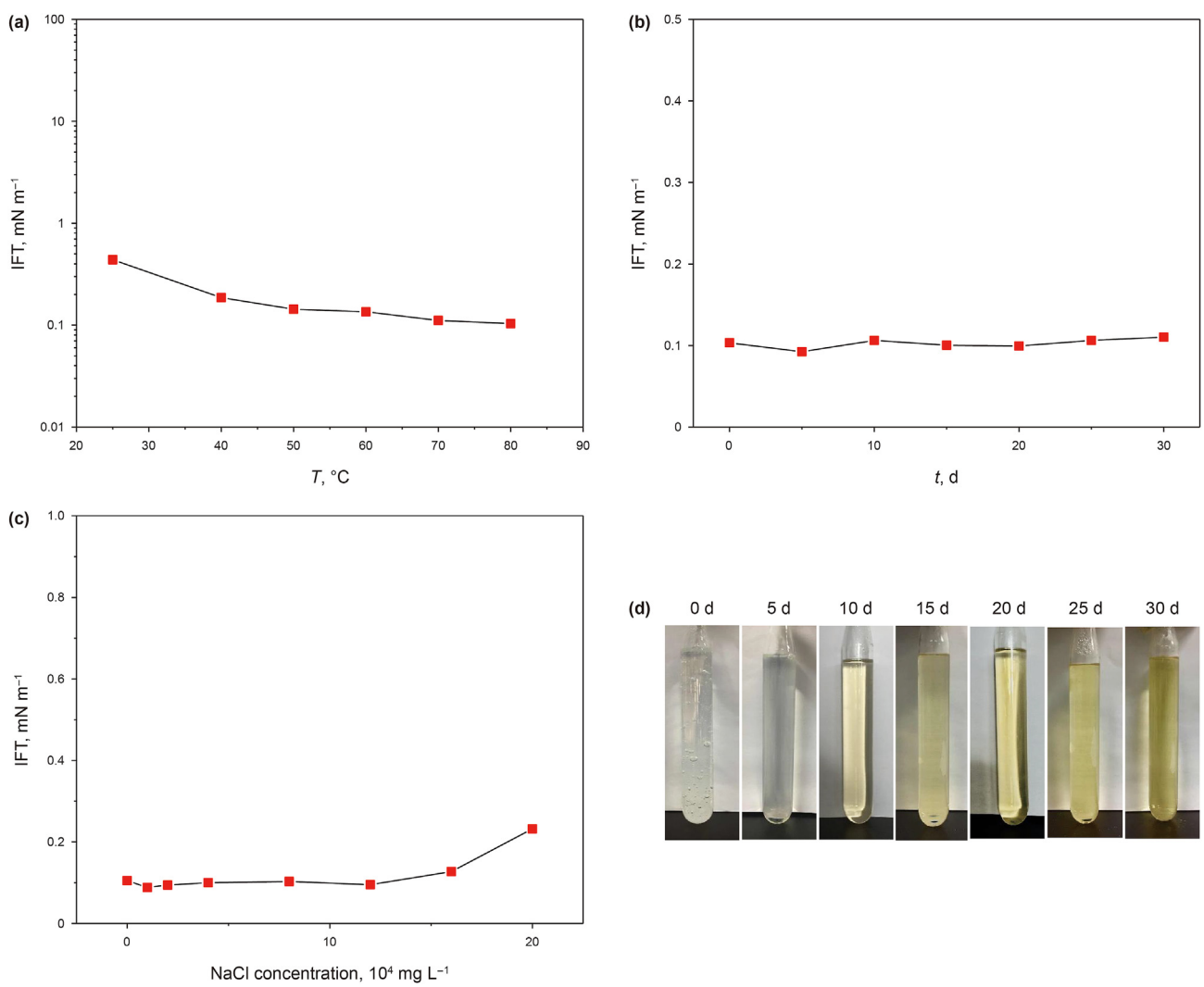

Fig. 8. The IFT between simulation oil and gel breaking fluid at different (**a**) temperatures, (**b**) aging time, (**c**) NaCl concentrations; (**d**) Pictures of gel breaking fluids for different aging time at 80 °C.

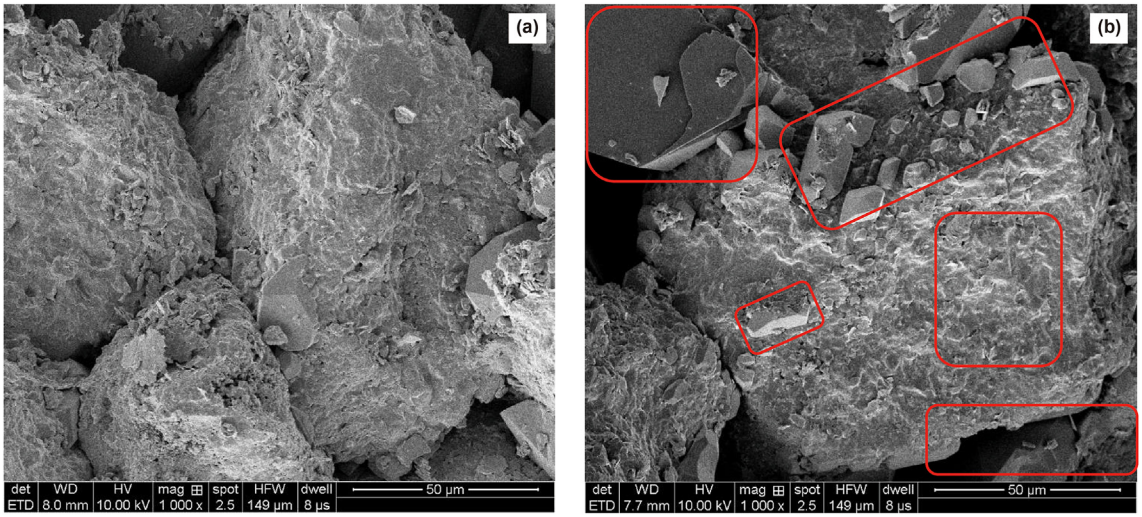

Fig. 9. The SEM pictures of core (**a**) before and (**b**) after spontaneous imbibition.

IFT, the gel breaking fluid with different concentrations of NaCl from 1×10^4 to 20×10^4 mg/L are prepared. The IFT between simulation oil and gel breaking fluid with varying degree of salinity at 80 °C is shown in Fig. 8c. The IFT is independent of salinity, indicating the good stability at high salinity.

We also use SEM to observe the surface morphology of saturated oil core before and after spontaneous imbibition as shown in Fig. 9. Thick oil slicks that adhere on the surface of the saturated core can be observed. The initial core also presents a rough surface. After spontaneous imbibition, some part of the smooth core surface is exposed, and the oil slicks on the core surface become thinner, indicating the oil stripping ability of breaking gel.

4. Conclusions

In summary, we develop a novel CO_2-, temperature-, pressure-triple responsive smart fluid by utilizing the "pseudo-Gemini" zwitterionic VES consisting of EHSB, TMEDA and NaPts without complex organic synthesis and purification. The introduction of CO_2 results in the protonation of tertiary amine groups in TMEDA, which is one of the main mechanisms of triple responsiveness. Protonated TMEDA molecules and EHSB molecules are "bridged" to form "pseudo-Gemini" zwitterionic VESs by non-covalent electrostatic attraction, resulting in longer and stiffer micelles. Due to the "pseudo-Gemini" zwitterionic VES, the thermal endurance of system with CO_2 is significantly better than that without CO_2. As the temperature increases, the viscosity drops rapidly due to the less protonation of TMEDA, weaker non-covalent interaction and stronger thermal motion. When the CO_2 partial pressure increases, higher CO_2 dissolution in aqueous solution facilitates the protonation of TMEDA, resulting in viscosity increase. The smart fluid is able to satisfy the technical requirement of tight oil fracturing construction at high temperature (140 °C) and pressure (3.5 MPa). Moreover, the gel breaking fluid shows excellent spontaneous imbibition oil expulsion (~40%), salt resistance (1.2×10^4 mg/L Na^+), temperature resistance (140 °C) and aging stability (30 days). The smart fluid, consisting of EHSB, TMEDA and NaPts, can not only meet the requirement of tight oil fracturing construction, but also make full use of fracturing energy and gel breaking fluids for oil expulsion, i.e., accomplishing tight oil fracturing-oil expulsion integration. It is remarkable that triple responsive smart fluid for tight oil fracturing-oil expulsion integration is presented for the first time in our work (Wu et al., 2018). Compared with the conventional Gemini surfactant system, the smart fluid based on "pseudo-Gemini" zwitterionic VES has better temperature resistance, while it has simpler synthesis routes and lower cost than the Gemini zwitterionic surfactant (Chu and Feng, 2010; Zhang et al., 2013; Feng and Chu, 2015; Zhou et al., 2019; Zhang et al., 2020; Li Z. et al., 2021). Therefore, it is envisioned that the triple responsive smart fluid for tight oil fracturing-oil expulsion integration is expected to open a new door to efficient tight oil exploitation and optimization.

Declaration of competing interest

The authors declare that they have no known competing financial interests or personal relationships that could have appeared to influence the work reported in this paper.

Acknowledgements

The authors sincerely appreciate the financial support from the National Key Research and Development Project (2019YFA0708700), the National Natural Science Foundation of China (51834010, 51874261, 51874337), the Key Research and Development Program of Shaanxi (2021GY-112), and a Discovery Grant from Natural Sciences and Engineering Research Council of Canada (NSERC RGPIN-2017-05080). The authors acknowledge China Scholarship Council (CSC) for the financial support provided to Mingwei Gao.

Appendix A. Supplementary data

Supplementary data to this article can be found online at https://doi.org/10.1016/j.petsci.2023.01.008.

References

Acharya, D.P., Kunieda, H., 2006. Wormlike micelles in mixed surfactant solutions. Adv. Colloid Interface Sci. 123–126, 401–413. https://doi.org/10.1016/j.cis.2006.05.024.

Bai, Y., Xiong, C., Shang, X., Xin, Y., 2014. Experimental study on ethanolamine/surfactant flooding for enhanced oil recovery. Energy Fuels 28, 1829–1837. https://doi.org/10.1021/ef402313n.

Bandyopadhyay, R., Sood, A.K., 2003. Effect of screening of intermicellar interactions on the linear and nonlinear rheology of a viscoelastic gel. Langmuir 19, 3121–3127. https://doi.org/10.1021/la0203741.

Baragau, I.-A., Lu, Z., Power, N.P., Morgan, D.J., Bowen, J., Diaz, P., Kellici, S., 2021.

Continuous hydrothermal flow synthesis of S-functionalised carbon quantum dots for enhanced oil recovery. Chem. Eng. J. 405, 126631. https://doi.org/10.1016/j.cej.2020.126631.
Chu, Z., Feng, Y., 2013. Vegetable-derived long-chain surfactants synthesized via a "green" route. ACS Sustainable Chem. Eng. 1, 75–79. https://doi.org/10.1021/sc300037e.
Chu, Z., Feng, Y., 2010. pH-switchable wormlike micelles. Chem. Commun. 46, 9028–9030. https://doi.org/10.1039/C0CC02415E.
Crews, J.B., 2005. Internal phase breaker technology for viscoelastic surfactant gelled fluids. In: SPE International Symposium on Oilfield Chemistry. Society of Petroleum Engineers. https://doi.org/10.2118/93449-MS.
Dai, C., Wang, K., Liu, Y., Li, H., Wei, Z., Zhao, M., 2015. Reutilization of fracturing flowback fluids in surfactant flooding for enhanced oil recovery. Energy Fuels 29, 2304–2311. https://doi.org/10.1021/acs.energyfuels.5b00507.
Dai, C., Wang, X., Li, Y., Lv, W., Zou, C., Gao, M., Zhao, M., 2017. Spontaneous imbibition investigation of self-dispersing silica nanofluids for enhanced oil recovery in low-permeability cores. Energy Fuels 31, 2663–2668. https://doi.org/10.1021/acs.energyfuels.6b03244.
Dai, C., Gao, M., Zhao, M., You, Q., Zhao, G., Wu, Y., Sun, Y., Li, L., Liu, Y., Liu, H., Wang, X., Guan, B., 2020. CO_2-sensitive Fracturing and Displacement Fluid and Method of Making the Same and Method for Fracturing and Displacement of Tight Oil Reservoir. US10584276B2.
Dong, B., Zheng, J., Zheng, L., Wang, S., Li, X., Inoue, T., 2008. Salt-induced viscoelastic wormlike micelles formed in surface active ionic liquid aqueous solution. J. Colloid Interface Sci. 319, 338–343. https://doi.org/10.1016/j.jcis.2007.11.040.
Ellis, R.C., 1998. An overview of frac packs: a technical revolution (evolution) process. J. Petrol. Technol. 50, 66–68. https://doi.org/10.2118/39232-JPT.
Feng, Y., Chu, Z., 2015. pH-Tunable wormlike micelles based on an ultra-long-chain "pseudo" Gemini surfactant. Soft Matter 11, 4614–4620. https://doi.org/10.1039/C5SM00677E.
Gao, M., Liu, P., Xue, Q., Zhao, M., Guo, X., You, Q., Dai, C., 2022. Non-ionic polar small molecules induced transition from elastic hydrogel via viscoelastic wormlike micelles to spherical micelles in zwitterionic surfactant systems. J. Mol. Liq. 359, 119343. https://doi.org/10.1016/j.molliq.2022.119343.
Granek, R., Cates, M.E., 1992. Stress relaxation in living polymers: results from a Poisson renewal model. J. Chem. Phys. 96, 4758–4767. https://doi.org/10.1063/1.462787.
Han, Y., Wang, Y., Meng, X., Wang, Q., Han, X., 2019. Wormlike micelles with a unique ladder shape formed by a C_{22}-tailed zwitterionic surfactant bearing a bulky piperazine group. Soft Matter 15, 7644–7653. https://doi.org/10.1039/C9SM01358J.
Heitmann, N., Pitoni, E., Devia, F., Simone, R., 2001. Polymer-free fluid technology optimizes seawater fracturing. In: Offshore Mediterranean Conference and Exhibition. Society of Petroleum Engineers.
Heldebrant, D.J., Jessop, P.G., Thomas, C.A., Eckert, C.A., Liotta, C.L., 2005. The reaction of 1,8-diazabicyclo[5.4.0]undec-7-ene (DBU) with carbon dioxide. J. Org. Chem. 70 (13), 5335–5338. https://doi.org/10.1021/jo0503759.
Holtsclaw, J., Funkhouser, G.P., 2010. A crosslinkable synthetic-polymer system for high-temperature hydraulic-fracturing applications. SPE Drill. Complet. 25, 555–563. https://doi.org/10.2118/125250-PA.
Hua, B., Zhai, H., Mu, L., Wang, Z., Chang, Y., Lan, J., 2020. U.S. Tight oil production tendency analysis. In: International Field Exploration and Development Conference 2019. Springer Series in Geomechanics and Geoengineering. https://doi.org/10.1007/978-981-15-2485-1_64.
Huang, F., Pu, C., Gu, X., Ye, Z., Liu, J., 2021. Study of a low-damage efficient-imbibition fracturing fluid without flowback used for low-pressure tight reservoirs. Energy 222, 119941. https://doi.org/10.1016/j.energy.2021.119941.
Khair, E.M.M., Shicheng, Z., Shanbo, M., Mei, Z., 2011. Performance and application of new anionic D3F-AS05 viscoelastic fracturing fluid. J. Pet. Sci. Eng. 78, 131–138. https://doi.org/10.1016/j.petrol.2011.05.011.
Kim, T.H., Cho, J., Lee, K.S., 2017. Evaluation of CO_2 injection in shale gas reservoirs with multi-component transport and geomechanical effects. Appl. Energy 190, 1195–1206. https://doi.org/10.1016/j.apenergy.2017.01.047.
Kong, F., Chen, J., Wang, H., Liu, X., Wang, X., Wen, X., Chen, C., Xie, Y.F., 2017. Application of coagulation-UF hybrid process for shale gas fracturing flowback water recycling: performance and fouling analysis. J. Membr. Sci. 524, 460–469. https://doi.org/10.1016/j.memsci.2016.11.039.
Kumar, R., Raghavan, S.R., 2009. Photogelling fluids based on light-activated growth of zwitterionic wormlike micelles. Soft Matter 5, 797–803. https://doi.org/10.1039/B809452G.
Kumar, R., Kalur, G.C., Ziserman, L., Danino, D., Raghavan, S.R., 2007. Wormlike micelles of a C_{22}-tailed zwitterionic betaine surfactant: from viscoelastic solutions to elastic gels. Langmuir 23, 12849–12856. https://doi.org/10.1021/la7028559.
Lerouge, S., Berret, J.-F., 2010. Shear-induced transitions and instabilities in surfactant wormlike micelles. In: Dusek, K., Joanny, J.-F. (Eds.), Polymer Characterization: Rheology, Laser Interferometry, Electrooptics. Springer Berlin Heidelberg, Berlin, Germany, pp. 1–71. https://doi.org/10.1007/12_2009_13.
Li, J., Zhao, M., Zheng, L., 2012. Salt-induced wormlike micelles formed by *N*-alkyl-*N*-methylpyrrolidinium bromide in aqueous solution. Colloids Surf., A 396, 16–21. https://doi.org/10.1016/j.colsurfa.2011.12.019.
Li, W., Nan, Y., You, Q., Jin, Z., 2021. CO_2 solubility in brine in silica nanopores in relation to geological CO_2 sequestration in tight formations: effect of salinity and pH. Chem. Eng. J. 411, 127626. https://doi.org/10.1016/j.cej.2020.127626.
Li, Z., Kang, W., Zhao, Y., Yang, H., Aidarova, S., 2021. Organic acid-enhanced viscoelastic surfactant and its application in fracturing fluids. Energy Fuels 35, 3130–3139. https://doi.org/10.1021/acs.energyfuels.0c04241.
Liu, D., Li, J., Zou, C., Cui, H., Ni, Y., Liu, J., Wu, W., Zhang, L., Coyte, R., Kondash, A., Vengosh, A., 2020. Recycling flowback water for hydraulic fracturing in Sichuan Basin, China: implications for gas production, water footprint, and water quality of regenerated flowback water. Fuel 272, 117621. https://doi.org/10.1016/j.fuel.2020.117621.
Lu, H., Zheng, C., Xue, M., Huang, Z., 2016. pH-regulated surface properties and pH-reversible micelle transition of a zwitterionic Ggemini surfactant in aqueous solution. Phys. Chem. Chem. Phys. 18, 32192–32197. https://doi.org/10.1039/C6CP06599F.
Lu, Y., Yang, F., Ge, Z., Wang, Q., Wang, S., 2017. Influence of viscoelastic surfactant fracturing fluid on permeability of coal seams. Fuel 194, 1–6. https://doi.org/10.1016/j.fuel.2016.12.078.
Mani, F., Peruzzini, M., Stoppioni, P., 2006. CO_2 absorption by aqueous NH_3 solutions: speciation of ammonium carbamate, bicarbonate and carbonate by a ^{13}C NMR study. Green Chem. 8, 995–1000. https://doi.org/10.1039/B602051H.
Mao, J., Yang, X., Chen, Y., Zhang, Z., Zhang, C., Yang, B., Zhao, J., 2018. Viscosity reduction mechanism in high temperature of a Gemini viscoelastic surfactant (VES) fracturing fluid and effect of counter-ion salt (KCl) on its heat resistance. J. Pet. Sci. Eng. 164, 189–195. https://doi.org/10.1016/j.petrol.2018.01.052.
Mao, J., Yang, X., Wang, D., Li, Y., Zhao, J., 2016. A novel Gemini viscoelastic surfactant (VES) for fracturing fluids with good temperature stability. RSC Adv. 6, 88426–88432. https://doi.org/10.1039/C6RA17823E.
Menger, F.M., Keiper, J.S., 2000. Gemini surfactants. Angew. Chem., Int. Ed. 39 (11), 1906–1920. https://doi.org/10.1002/1521-3773(20000602)39:11<1906::AID-ANIE1906>3.0.CO;2-Q.
Miskimins, J.L., 2009. Design and life-cycle considerations for unconventional reservoir wells. SPE Prod. Oper. 24, 353–359. https://doi.org/10.2118/114170-PA.
Miyoshi, E., Nishinari, K., 1999. Non-Newtonian flow behaviour of gellan gum aqueous solutions. Colloid Polym. Sci. 277, 727–734. https://doi.org/10.1007/s003960050446.
Mushi, S.J., Kang, W., Yang, H., Wang, P., Hou, X., 2020. Viscoelasticity and microstructural properties of zwitterionic surfactant induced by hydroxybenzoate salt for fracturing. J. Mol. Liq. 301, 112485. https://doi.org/10.1016/j.molliq.2020.112485.
Nagarajan, R., 2002. Molecular packing parameter and surfactant self-assembly: the neglected role of the surfactant tail. Langmuir 18, 31–38. https://doi.org/10.1021/la010831y.
Peng, S., Liu, Y., Ko, L.T., Ambrose, W., 2019. Water/oil displacement by spontaneous imbibition through multiscale imaging and implication on wettability in Wolfcamp shale. In: SPE/AAPG/SEG Unconventional Resources Technology Conference. Society of Petroleum Engineers. https://doi.org/10.15530/urtec-2019-194.
Raghavan, S.R., Douglas, J.F., 2012. The conundrum of gel formation by molecular nanofibers, wormlike micelles, and filamentous proteins: gelation without cross-links? Soft Matter 8, 8539–8546. https://doi.org/10.1039/C2SM25107H.
Rassenfoss, S., 2011. From flowback to fracturing: water recycling grows in the Marcellus shale. J. Petrol. Technol. 63, 48–51. https://doi.org/10.2118/0711-0048-JPT.
Samuel, M., Card, R.J., Nelson, E.B., Brown, J.E., Vinod, P.s., Temple, H.L., Qu, Q., Fu, D.K., 1997. Polymer-free fluid for hydraulic fracturing. In: SPE Annual Technical Conference and Exhibition. Society of Petroleum Engineers. https://doi.org/10.2118/38622-MS.
Sheng, J.J., 2020. Chapter seven - water injection. In: Sheng, J.J. (Ed.), Enhanced Oil Recovery in Shale and Tight Reservoirs. Gulf Professional Publishing, Houston, Texas, pp. 151–171. https://doi.org/10.1016/B978-0-12-815905-7.00007-4.
Sheng, J., Li, L., Yu, Y., Meng, X., Sharma, S., Huang, S., Shen, Z., Zhang, Y., Wang, X., Carey, B., Nguyen, P., Porter, M., Jimenez, M.J., Viswanathan, H., Mody, F., Barnes, W., Cook, T., Griffith, P., 2017. Maximize Liquid Oil Production from Shale Oil and Gas Condensate Reservoirs by Cyclic Gas Injection. https://doi.org/10.2172/1427584.
Someya, S., Bando, S., Chen, B., Song, Y., Nishio, M., 2005. Measurement of CO_2 solubility in pure water and the pressure effect on it in the presence of clathrate hydrate. Int. J. Heat Mass Tran. 48, 2503–2507. https://doi.org/10.1016/j.ijheatmasstransfer.2004.12.043.
Wang, F., Yang, K., You, J., Lei, X., 2019. Analysis of pore size distribution and fractal dimension in tight sandstone with mercury intrusion porosimetry. Results Phys. 13, 102283. https://doi.org/10.1016/j.rinp.2019.102283.
Wang, J., Liang, M., Tian, Q., Feng, Y., Yin, H., Lu, G., 2018. CO_2-switchable foams stabilized by a long-chain viscoelastic surfactant. J. Colloid Interface Sci. 523, 65–74. https://doi.org/10.1016/j.jcis.2018.03.090.
Wang, L., Long, Y., Ding, H., Geng, J., Bai, B., 2017. Mechanically robust recrosslinkable polymeric hydrogels for water management of void space conduits containing reservoirs. Chem. Eng. J. 317, 952–960. https://doi.org/10.1016/j.cej.2017.02.140.
Wang, T., Xiao, J., Wang, L., Ma, A., Tian, M., Wang, C., 2020. Synthesis of Gemini ammonium sulfobetaine and its proppant suspension and gel-breaking mechanisms. RSC Adv. 10, 7879–7886. https://doi.org/10.1039/D0RA00211A.
Wei, B., Lu, L., Pu, W., Wu, R., Zhang, X., Li, Y., Jin, F., 2017. Production dynamics of CO_2 cyclic injection and CO_2 sequestration in tight porous media of Lucaogou formation in Jimsar sag. J. Pet. Sci. Eng. 157, 1084–1094. https://doi.org/10.1016/j.petrol.2017.08.023.
Wei, B., Zhang, X., Liu, J., Xu, X., Pu, W., Bai, M., 2020. Adsorptive behaviors of supercritical CO_2 in tight porous media and triggered chemical reactions with

rock minerals during CO_2-EOR and -sequestration. Chem. Eng. J. 381, 122577. https://doi.org/10.1016/j.cej.2019.122577.
Wu, X., Huang, Y., Fang, S., Dai, C., Li, H., Xu, Z., Zhao, M., 2018b. CO_2-responsive smart wormlike micelles based on monomer and "pseudo" Gemini surfactant. J. Ind. Eng. Chem. 60, 348–354. https://doi.org/10.1016/j.jiec.2017.11.021.
Wu, X., Zhang, Y., Sun, X., Huang, Y., Dai, C., Zhao, M., 2018a. A novel CO_2 and pressure responsive viscoelastic surfactant fluid for fracturing. Fuel 229, 79–87. https://doi.org/10.1016/j.fuel.2018.04.081.
Xu, T., Mao, J., Zhang, Y., Yang, X., Lin, C., Du, A., Zhang, H., 2021. Application of Gemini viscoelastic surfactant with high salt in brine-based fracturing fluid. Colloids Surf., A 611, 125838. https://doi.org/10.1016/j.colsurfa.2020.125838.
Yan, C., Pochan, D.J., 2010. Rheological properties of peptide-based hydrogels for biomedical and other applications. Chem. Soc. Rev. 39, 3528–3540. https://doi.org/10.1039/b919449p.
Yang, C., Hu, Z., Song, Z., Bai, J., Zhang, Y., Luo, J., Du, Y., J, Q., 2017b. Self-assembly properties of ultra-long-chain Gemini surfactant with high performance in a fracturing fluid application. J. Appl. Polym. Sci. 134 (11), 44602. https://doi.org/10.1002/app.44602.
Yang, C., Song, Z., Zhao, J., Hu, Z., Zhang, Y., Jiang, Q., 2017a. Self-assembly properties of ultra-long-chain Gemini surfactants bearing multiple amide groups with high performance in fracturing fluid application. Colloids Surf., A 523, 62–70. https://doi.org/10.1016/j.colsurfa.2017.03.062.
Yang, Z., Li, X., Li, D., Yin, T., Zhang, P., Dong, Z., Lin, M., Zhang, J., 2019. New Method Based on CO_2-switchable wormlike micelles for controlling CO_2 breakthrough in a tight fractured oil reservoir. Energy Fuels 33, 4806–4815. https://doi.org/10.1021/acs.energyfuels.9b00362.
Yin, H., Feng, Y., Li, P., Doutch, J., Han, Y., Mei, Y., 2019. Cryogenic wormlike micelles. Soft Matter 15, 2511–2516. https://doi.org/10.1039/C9SM00068B.
Zhang, T., Li, Z., Gao, M., Xu, Z., Adenutsi, C.D., You, Q., 2022b. New insights into the synergism between silica nanoparticles and surfactants on interfacial properties: implications for spontaneous imbibition in tight oil reservoirs. J. Pet. Sci. Eng. 215, 110647. https://doi.org/10.1016/j.petrol.2022.110647.
Zhang, T.-T., Li, Z.-P., Adenutsi, C.D., Wei, Y.-Z., Ma, Z.-F., You, Q., 2022a. Quantitativae investigation of nanofluid imbibition in tight oil reservoirs based on NMR technique. Petrol. Sci. 19 (5), 2185–2198. https://doi.org/10.1016/j.petsci.2022.04.013.
Zhang, W., Mao, J., Yang, X., Zhang, H., Zhang, Z., Yang, B., Zhang, Y., Zhao, J., 2018. Study of a novel Gemini viscoelastic surfactant with high performance in clean fracturing fluid application. Polymer 10 (11), 1215. https://doi.org/10.3390/polym10111215.
Zhang, W., Mao, J., Yang, X., Zhang, H., Zhao, J., Tian, J., Lin, C., Mao, J., 2019. Development of a sulfonic Gemini zwitterionic viscoelastic surfactant with high salt tolerance for seawater-based clean fracturing fluid. Chem. Eng. Sci. 207, 688–701. https://doi.org/10.1016/j.ces.2019.06.061.
Zhang, Y., Feng, Y., Wang, Y., Li, X., 2013. CO_2-switchable viscoelastic fluids based on a pseudogemini surfactant. Langmuir 29, 4187–4192. https://doi.org/10.1021/la400051a.
Zhang, Y., Kong, W., An, P., He, S., Liu, X., 2016. CO_2/pH-controllable viscoelastic nanostructured fluid based on stearic acid soap and bola-type quaternary ammonium salt. Langmuir 32, 2311–2320. https://doi.org/10.1021/acs.langmuir.5b04459.
Zhang, Y., Mao, J., Zhao, J., Yang, X., Zhang, H., 2018. Preparation of a novel ultra-high temperature low-damage fracturing fluid system using dynamic crosslinking strategy. Chem. Eng. J. 354, 913–921. https://doi.org/10.1016/j.cej.2018.08.021.
Zhang, Y., Mao, J., Zhao, J., Zhang, W., Liao, Z., Xu, T., Du, A., Zhang, Z., Yang, X., Ni, Y., 2020. Preparation of a novel sulfonic Gemini zwitterionic viscoelastic surfactant with superior heat and salt resistance using a rigid-soft combined strategy. J. Mol. Liq. 318, 114057. https://doi.org/10.1016/j.molliq.2020.114057.
Zhao, M., Gao, M., Dai, C., Zou, C., Yang, Z., Wu, X., Liu, Y., Wu, Y., Fang, S., Lv, W., 2017. Investigation of novel triple-responsive wormlike micelles. Langmuir 33, 4319–4327. https://doi.org/10.1021/acs.langmuir.7b01011.
Zhou, F., Su, H., Liang, X., Meng, L., Yuan, L., Li, X., Liang, T., 2019. Integrated hydraulic fracturing techniques to enhance oil recovery from tight rocks. Petrol. Explor. Dev. 46, 1065–1072. https://doi.org/10.1016/S1876-3804(19)60263-6.
Zhou, J., Jin, Z., Luo, K.H., 2020. The role of brine in gas adsorption and dissolution in kerogen nanopores for enhanced gas recovery and CO_2 sequestration. Chem. Eng. J. 399, 125704. https://doi.org/10.1016/j.cej.2020.125704.